

JGR Biogeosciences

RESEARCH ARTICLE

10.1029/2019JG005621

Key Points:

- The influence of aerobic methane oxidation on carbon dioxide and pH is investigated the U.S. Mid-Atlantic Bight
- A small fraction of ancient-methane derived carbon is assimilated into the dissolved inorganic carbon
- Oxidation of ancient methane-derived carbon could contribute to deepwater acidification over longer time scales

Supporting Information:

- Supporting Information S1

Correspondence to:

F. Garcia-Tigreros,
fenix.garcia.tigreros@gmail.com

Citation:

Garcia-Tigreros, F., Leonte, M., Ruppel, C. D., Ruiz-Angulo, A., Joung, D. J., Young, B., & Kessler, J. D. (2021). Estimating the impact of seep methane oxidation on ocean pH and dissolved inorganic radiocarbon along the U.S. Mid-Atlantic Bight. *Journal of Geophysical Research: Biogeosciences*, 126, e2019JG005621. <https://doi.org/10.1029/2019JG005621>

Received 27 DEC 2019

Accepted 5 NOV 2020

Accepted article online 23 DEC 2020

Estimating the Impact of Seep Methane Oxidation on Ocean pH and Dissolved Inorganic Radiocarbon Along the U.S. Mid-Atlantic Bight

Fenix Garcia-Tigreros^{1,2} , Mihai Leonte¹ , Carolyn D. Ruppel³ , Angel Ruiz-Angulo⁴ , Dong Joo Joung¹ , Benjamin Young¹ , and John D. Kessler¹ 

¹Department of Earth and Environmental Sciences, University of Rochester, Rochester, NY, USA, ²Now at the Department of Environmental and Forest Sciences, University of Washington, Seattle, WA, USA, ³U.S. Geological Survey, Woods Hole, MA, USA, ⁴Icelandic Meteorological Office, Reykjavik, Iceland

Abstract Ongoing ocean warming can release methane (CH₄) currently stored in ocean sediments as free gas and gas hydrates. Once dissolved in ocean waters, this CH₄ can be oxidized to carbon dioxide (CO₂). While it has been hypothesized that the CO₂ produced from aerobic CH₄ oxidation could enhance ocean acidification, a previous study conducted in Hudson Canyon shows that CH₄ oxidation has a small short-term influence on ocean pH and dissolved inorganic radiocarbon. Here we expand upon that investigation to assess the impact of widespread CH₄ seepage on CO₂ chemistry and possible accumulation of this carbon injection along 234 km of the U.S. Mid-Atlantic Bight. Consistent with the estimates from Hudson Canyon, we demonstrate that a small fraction of ancient CH₄-derived carbon is being assimilated into the dissolved inorganic radiocarbon (mean fraction of 0.5 ± 0.4%). The areas with the highest fractions of ancient carbon coincide with elevated CH₄ concentration and active gas seepage. This suggests that aerobic CH₄ oxidation has a greater influence on the dissolved inorganic pool in areas where CH₄ concentrations are locally elevated, instead of displaying a cumulative effect downcurrent from widespread groupings of CH₄ seeps. A first-order approximation of the input rate of ancient-derived dissolved inorganic carbon (DIC) into the waters overlying the northern U.S. Mid-Atlantic Bight further suggests that oxidation of ancient CH₄-derived carbon is not negligible on the global scale and could contribute to deepwater acidification over longer time scales.

Plain Language Summary Ocean acidity may be enhanced not only due to the oceanic uptake of atmospheric carbon dioxide but also through temperature-driven processes that can mobilize ancient carbon stores and generate additional carbon dioxide. One of these processes is the oxidation of methane derived from seafloor seepage. Here, we investigate if the widespread release and subsequent oxidation of seep methane into carbon dioxide could contribute to the acidification of deep waters along the U.S. Mid-Atlantic Bight. Our results suggest that over short time scales, methane's role in enhancing ocean acidification is small. However, over longer time periods, methane-derived carbon could contribute to deepwater acidification.

1. Introduction

A significant fraction of the carbon dioxide (CO₂) emitted to the atmosphere since the preindustrial Holocene has been taken up by the oceans, leading to higher surface water CO₂ levels (Broecker et al., 1979; Canadell et al., 2007; Doney et al., 2009; Quay et al., 1992). While this uptake of anthropogenic CO₂ has helped mitigate atmospheric warming, the rate at which CO₂ is being taken up by the surface ocean is unprecedented over the past 66 million years (Zeebe et al., 2016) and is contributing to a pH decline in surface waters (Feely et al., 2004; Orr et al., 2005). Ocean acidification has received increasing attention due to its negative impact on calcifying organisms and ocean ecosystems (Doney et al., 2009; Feely et al., 2004; Orr et al., 2005). It has been estimated that since the Industrial Revolution, ocean pH has decreased by 0.1 units, and pH is predicted to decrease by another 0.3–0.4 units by the end of the 21st century (Feely et al., 2009).

While predictions only consider acidification due to the uptake of atmospheric CO₂, other natural and anthropogenic processes can interact to exacerbate local pH decline. In addition to rising atmospheric CO₂ uptake, eutrophication in coastal regions and the degradation of terrestrial organic carbon in Arctic

coastal shelves have been recognized as processes that further increase seawater CO₂ (Alling et al., 2012; Cai et al., 2011; Feely et al., 2010; Semiletov et al., 2016; Sunda & Cai, 2012). Similarly, aerobic microbial oxidation of methane (CH₄) produces CO₂ and could increase the acidity of bottom waters (Biaostoch et al., 2011; Boudreau et al., 2015; Ruppel, 2011; Zachos et al., 2005).

Marine continental slopes hold the largest climate-sensitive CH₄ reservoirs in the form of gas hydrates and are currently susceptible to degradation due to warming waters (Ciais et al., 2013; Kvenvolden, 1988; Phrampus & Hornbach, 2012; Ruppel, 2011; Ruppel & Kessler, 2017; Stranne et al., 2016). It has been estimated that warming of bottom waters under a global warming scenario where CO₂ increases yearly by 1% could destabilize gas hydrate deposits and inject 560 to 2,140 Tg yr⁻¹ of CH₄ into ocean waters (Lamarque, 2008). Despite the initial view that CH₄ emitted from the seafloor would escape to the atmosphere and enhance global warming (Archer et al., 2009; Krey et al., 2009; Kvenvolden et al., 2001), recent studies show that most CH₄ stays in the water column, alleviating the direct impact of this greenhouse gas on climate (e.g., Lamarque, 2008; Leonte et al., 2017, 2020; McGinnis et al., 2006; Ruppel & Kessler, 2017). However, dissolved CH₄ is efficiently oxidized to carbon dioxide (CO₂) by methanotrophic archaea and bacteria (e.g., Chan et al., 2019; Du & Kessler, 2012; Kessler et al., 2011; Leonte et al., 2017; Mau et al., 2012; Valentine et al., 2001) which could potentially affect ocean inorganic carbon chemistry and enhance ocean acidification (Biaostoch et al., 2011; Boudreau et al., 2015; Ruppel, 2011; Zachos et al., 2005).

The dissolved inorganic carbon (DIC) reservoir in seawater is one of the largest reservoirs of carbon on Earth (~38,000 Pg C; Ciais et al., 2013) and provides a strong buffer to changes in oceanic pH. As a result, changes in pH smaller than those associated with the seasonal variations in primary production and respiration may be difficult to detect, unless the input of CO₂ is so large as to influence the DIC mass balance on either short- or longer-term time scales. The drawdown of anthropogenic CO₂ into the surface ocean is one prominent example of a long-term CO₂ perturbation influencing DIC and pH. A geologic event that is often used as an analog to understand the impacts of massive carbon release on the Earth system is the Paleocene-Eocene Thermal Maximum (PETM; Dickens et al., 1995; Zeebe et al., 2016). Some paleoclimate studies suggest that during the PETM (~56 Myr ago), the aggressive release of 110 to 1,500 Tg yr⁻¹ of hydrate derived-CH₄ resulted in significant changes in ocean chemistry and the global carbon cycle (Dickens, 2003; Dickens et al., 1995; Kennett & Stott, 1991). Estimates of contemporary global CH₄ release rates from all potential seafloor sources into ocean waters range between 16 and 3,200 Tg CH₄ yr⁻¹ (Ruppel & Kessler, 2017). While this is a large and uncertain range, the middle to upper range is of similar magnitude to that estimated for the PETM.

Garcia-Tigreros and Kessler (2018) investigated acute influences of aerobic CH₄ oxidation on pH and DIC in the upper Hudson Canyon, a 50-km-long shelf break canyon with restricted circulation and riverine and terrestrial carbon inputs. Results from that study indicate that CH₄ oxidation had a limited influence on pH and DIC within the active CH₄ seep field found in the canyon over short time scales. However, Garcia-Tigreros and Kessler (2018) also suggested that CO₂ derived from CH₄ oxidation might accumulate to have a more significant influence over decadal time scales or longer. In the absence of conducting decades-long measurement campaigns to potentially observe this signal, the study here focuses on water masses that flow southward across a corridor of hundreds of CH₄ seeps arrayed along more than 234 linear kilometers of the upper slope in the U.S. Mid-Atlantic Bight (MAB). We leverage the southward flow of ocean currents in this region to test whether the sequential inputs of seep CH₄, which are then oxidized to CO₂, will lead to a cumulative input and impact DIC concentration and pH.

2. Methods

2.1. Study Location

The northern U.S. MAB between Baltimore Canyon and Cape Hatteras (Figure 1) was chosen as an ideal region to assess the accumulation of DIC sourced from the oxidation of seep CH₄. This area is recognized for its relatively dense distribution of CH₄ seeps (over 300 seafloor gas seeps), most of which lie on the upper continental slope at water depths of 250 to 600 m (Skarke et al., 2014). This depth range includes the landward limit of gas hydrate stability (~550–575 m; Brothers et al., 2014). The Gulf Stream, the northward

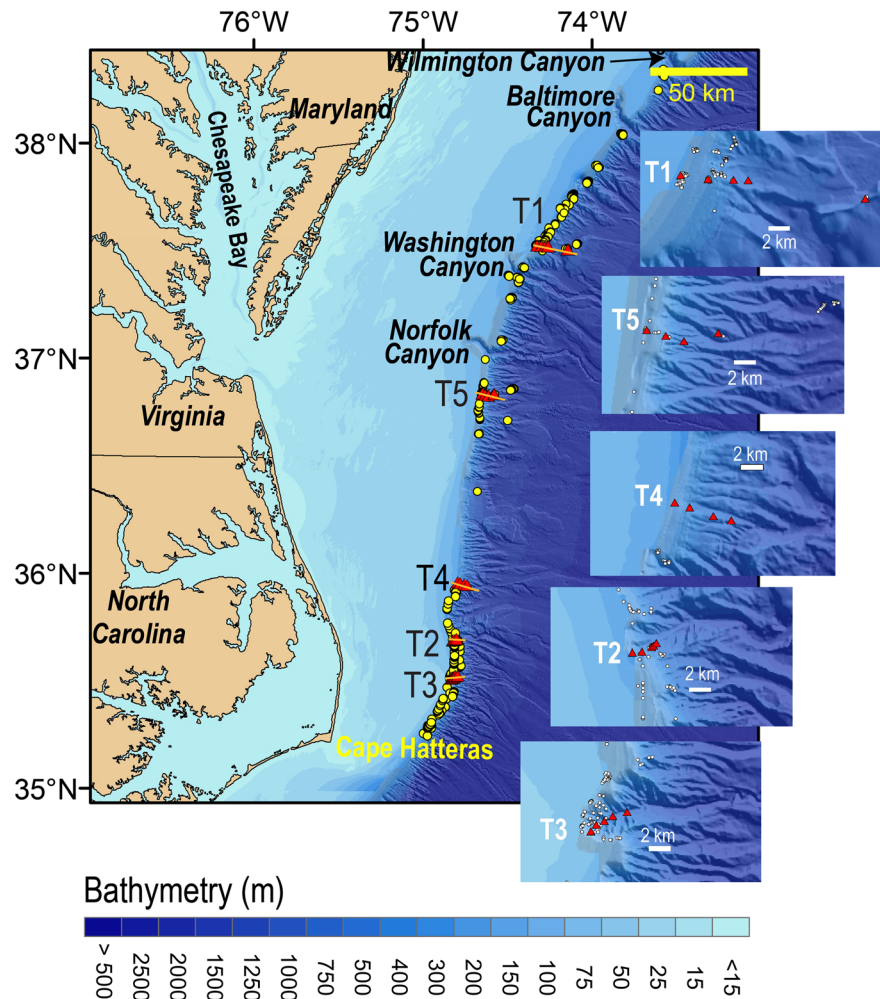


Figure 1. Study area showing Transects T1 through T5. Inset maps show a detailed view of the stations' bathymetry and locations (red triangles). Bathymetry data were obtained from Andrews et al. (2013). Yellow circles show gas seeps previously identify by Skarke et al. (2014) and detected during this research (Baldwin et al., 2020).

flowing western boundary current for the North Atlantic basin, separates from the continental slope around Cape Hatteras and veers northeastward away from the New England margin (Fratantoni & Pickart, 2007; Rasmussen et al., 2005). Landward of the Gulf Stream, the upper slope current generally flows southward across the clusters of dense seeps, facilitating the cumulative input of CH₄-derived DIC as currents carry water from north to south (Figure 2).

2.2. Sample Collection and Methods

Water samples for this study were acquired from Niskin bottles during conductivity-temperature-depth (CTD) casts from the R/V *Hugh R. Sharp* between 25 August and 3 September 2017. The R/V *Hugh R. Sharp* was confirmed to be a ¹⁴C-clean ship by following the swipe protocols from the W. M. Keck Carbon Cycle Accelerator Mass Spectrometry (UCI KCCAMS) facility at the University of California, Irvine. The CTD casts were conducted along five MAB transects oriented roughly perpendicular to the shelf break and stretching from the upper slope (136–170 m) to ~1,000 m water depth. Five CTD stations were selected on each transect, and samples were collected throughout the water column from the near-surface waters (~2 m depth) to within 5 m of the seafloor, when possible. Transect and station locations relative to seafloor gas seeps were guided by water column imaging data collected by the U.S. Geological Survey (USGS) using a Simrad EK60 broadband fisheries echosounder with a 38 kHz transducer. Approximately 12 samples were collected in the water column at the location of each CTD cast, for a total of 293 successful water samples

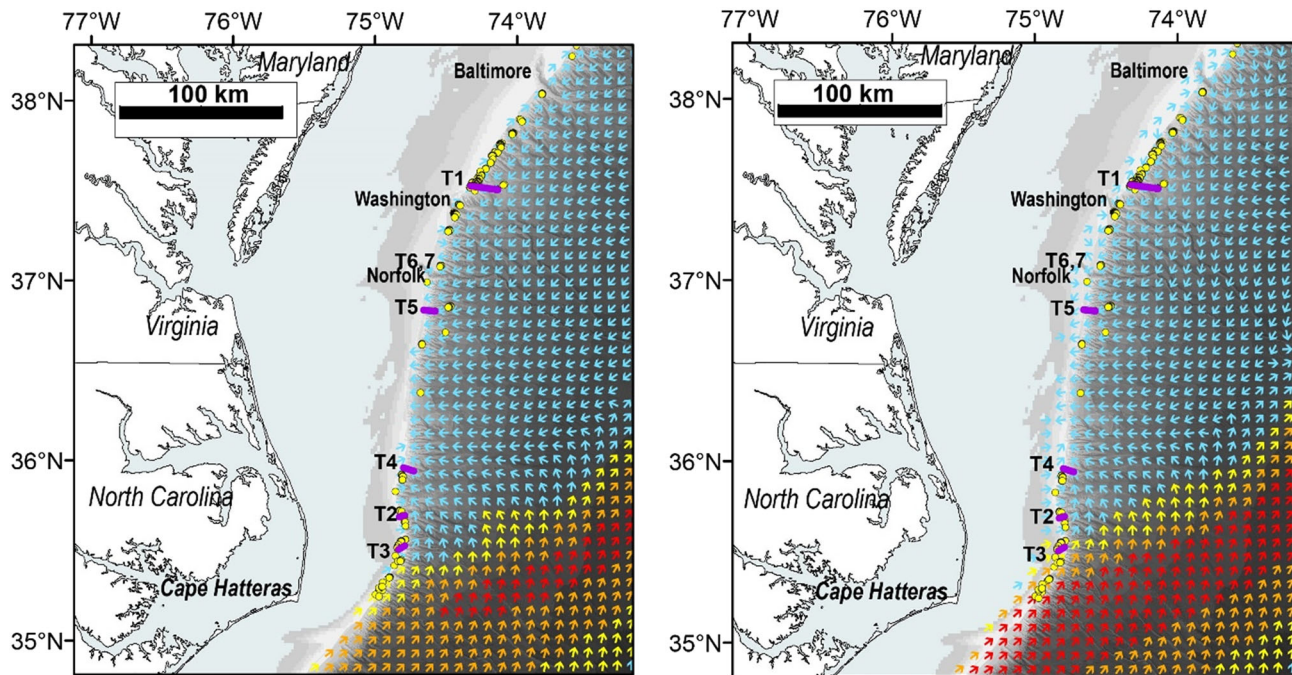


Figure 2. Average ocean current direction and magnitude at 200 m (left) and 400 m (right) depth in the study area from 1 to 3 September 2017 based on the USGS Coupled-Ocean-Atmosphere-Wave-Sediment-Transport model (Warner et al., 2010). These dates were chosen to coincide with most sample collections. Current speed is indicated by the color of the vectors, with red (center of Gulf Stream) denoting >1 m/s, orange 0.5 to 1 m/s, yellow 0.25 to 0.5 m/s, and blue 0 to 0.25 m/s. The locations of the CTD transects are indicated in purple. Yellow circles show gas seeps previously identified by Skarke et al. (2014) and detected during this research (Baldwin et al., 2020).

at the 25 stations. Temperature, salinity, and conductivity were recorded using a Sea-Bird Scientific 911 Plus and dissolved oxygen data was recorded using a Sea-Bird Scientific SBE 43 Dissolved Oxygen Sensor.

The water samples were analyzed for DIC concentration ($[DIC]$), DIC radiocarbon ($\Delta^{14}C-DIC$), stable isotopes of DIC ($\delta^{13}C-DIC$), pH, and CH_4 concentration. $[DIC]$ samples were collected by transferring water from Niskin bottles to combusted and pre-cleaned 120 ml serum vials (Wheaton) using Tygon tubing, then poisoned with 50 μ l of a 55 μ M $HgCl_2$ solution, and stored at 4°C until analysis, following the Standard Operating Procedure 1 in Dickson et al. (2007). $[DIC]$ samples were measured by acidification of 30 ml of water, and the subsequent release of CO_2 was quantified with a CO_2 cavity-ringdown spectrometer (CRDS; Picarro G1101-*i*). This method produced an accuracy and precision of ± 2 and ± 4 μ mol/kg, respectively, as determined by duplicate samples and repeat analysis of certified reference materials prepared at the Scripps Institution of Oceanography, University of California, San Diego.

Samples for pH were drawn directly from the Niskin bottle into a 10 cm path-length optical cylindrical cell from Starna Cells. Samples were measured spectrophotometrically on board the research vessel using an Agilent Cary 100 ultraviolet-visible (UV-Vis) spectrophotometer and m-cresol purple dye (Clayton & Byrne, 1993; Liu et al., 2011). The pH values are reported on the total scale with a precision better than 0.0002 based on duplicate measurements and an estimated accuracy better than 0.002. Dissolved CO_2 concentration ($[CO_2]$) was calculated based on $[DIC]$ and pH measurements using the MATLAB CO2SYS program (Van Heuven et al., 2011).

Natural $\Delta^{14}C-DIC$ and $\delta^{13}C-DIC$ samples were handled following the procedures from Gao et al. (2014). Briefly, $\Delta^{14}C-DIC$ and $\delta^{13}C-DIC$ samples were collected in combusted 60 ml borosilicate bottles, poisoned with 12 μ l of a 55 μ M mercuric chloride ($HgCl_2$) solution, sealed, and stored in the dark at room temperature until isotope analysis. $\Delta^{14}C-DIC$ aliquots >0.4 mg C were analyzed at the UCI KCCAMS facility with an accuracy and precision of 0.1‰ and 1.7‰, respectively (Gao et al., 2014; Pack et al., 2015). $\delta^{13}C-DIC$ samples were measured using a Finnigan Delta Plus stable isotope mass spectrometer, with a precision better than

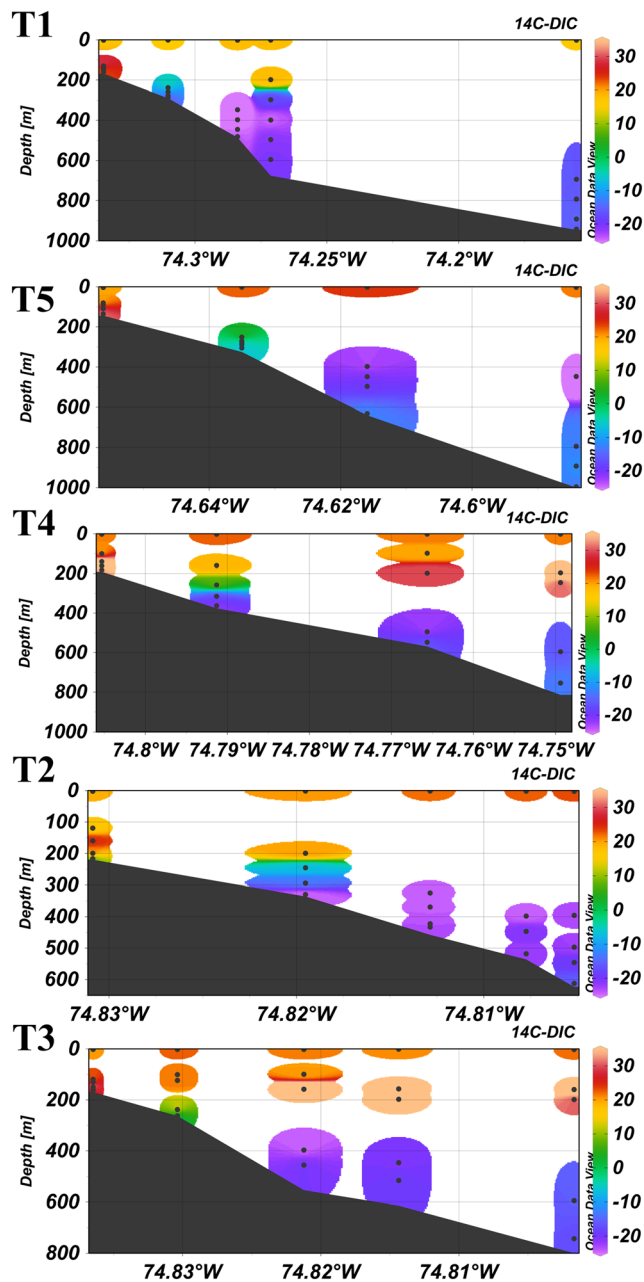


Figure 3. Distribution of $\Delta^{14}\text{C-DIC}$ (‰) for all sampled transects, from northernmost (T1) to southernmost (T3). Locations of discrete samples are indicated by black dots.

0.2‰. Of the discrete water samples collected, 125 were analyzed for $\Delta^{14}\text{C-DIC}$ and $\delta^{13}\text{C-DIC}$. Results are presented using the per mil notation (‰) and years before present (yr BP). Modern ages are defined here as carbon fixed from the atmosphere after 1950 and include $\Delta^{14}\text{C}$ -enriched CO_2 from nuclear weapons testing.

Methane concentration was measured concurrently on this expedition and generally followed the procedures outlined in Weinstein et al. (2016). On this expedition, seawater was collected from Niskin bottles into 250 ml glass bottles (Wheaton) using 1/4" Tygon tubing. Vials were filled from the bottom and water allowed to overflow in order to flush the vials with at least two volumes of water before capping with a butyl rubber stopper and aluminum crimp cap (Wheaton). Immediately after capping, a 10 ml ultrahigh purity nitrogen headspace was introduced into each vial via displacement and 250 μl of a saturated HgCl_2 solution was then added to each vial to halt further biological activity and preserve the samples until analysis. Methane concentration measurements were performed on board the research vessel using an Agilent 6850 gas chromatograph with a flame ionization detector (GC-FID) using a headspace equilibration technique. The uncertainty associated with these measurements was 2.5% based on replicate measurements.

2.3. Current Measurements

Water current velocities were taken by the USGS using an RDI Workhorse 300-kHz acoustic Doppler current profiler (ADCP) in a deepwater housing which was mounted inside the CTD carousel looking downward. The ADCP was lowered throughout the water column using the CTD carousel, and usable data were recorded during all CTD deployments except Transect T1 due to technical issues. The lowered ADCP (LADCP) data were processed with the Lamont Doherty Earth Observatory software package, version IX_13 (Thurnherr, 2011), using bottom tracking, GPS (from CTD time series), and data from the ship's hull mounted RDI Workhorse 300-kHz ADCP to constrain the inversion model. LADCP processing yielded north and east velocity components that were used to calculate the direction and speed of ocean currents at the time and location of sampling (Ruiz-Angulo et al., 2020).

2.4. Statistical Analysis

Statistical analyses were performed using MATLAB R2020a, unless otherwise stated. Data distribution was assessed using a Shapiro-Wilk normality test. For data that were non-normally distributed (Shapiro-Wilk: $p \leq 0.05$), comparisons were made using non-normally distributed Kruskal-Wallis test for more than two groups. Outliers were identified using bivariate comparisons of continuous data using the standard deviation method. Pearson correlation tests were conducted for normally distributed data and Spearman's correlation for nonparametric associations. The Mann-Whitney U test was used to determine statistical significance and significant correlations were reported as $p < 0.05$.

3. Results

Natural radiocarbon measurements of DIC for the data set ranged from -28.5‰ to 45.1‰ (165 yr BP to modern ages). Surface waters at all stations were enriched in $\Delta^{14}\text{C-DIC}$, which ranged between 15.5‰ and 24.1‰ (Figure 3 and Figure S1 in the supporting information). The highest $\Delta^{14}\text{C-DIC}$ values were observed in subsurface waters between 100 and 200 m ($17.1\text{--}45.1\text{‰}$). Below 200 m, $\Delta^{14}\text{C-DIC}$ values decrease rapidly, reaching a mean minimum value of -23.6‰ between 350 and 450 m (range = -28.5‰ to -20.6‰ , $n = 15$). For

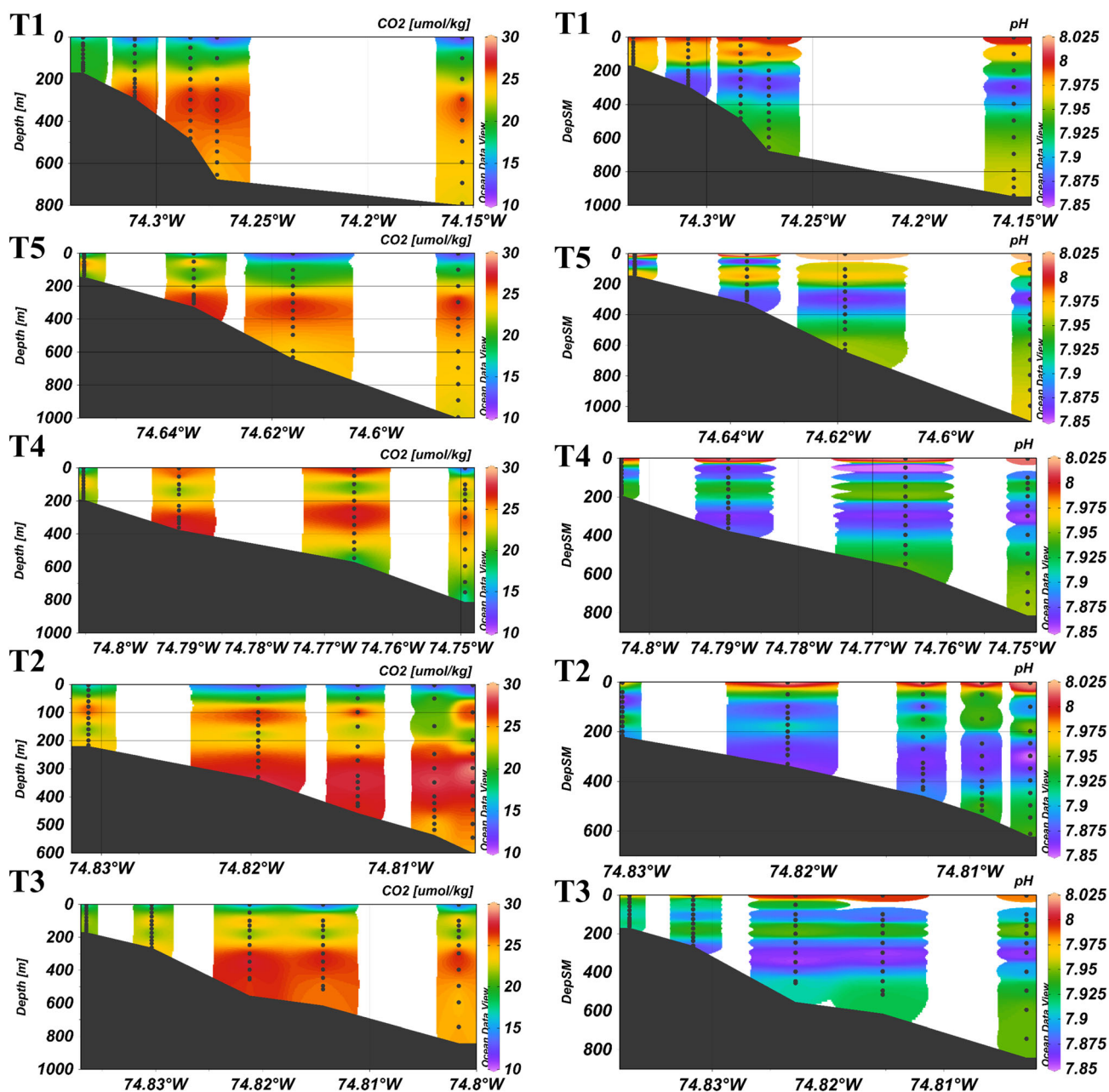


Figure 4. Distribution of $[CO_2]$ ($\mu\text{mol/kg}$) on left and pH on right along sampled transects, from northernmost (T1) to southernmost (T3). Locations of discrete samples are indicated by black dots.

depths greater than 600 m, values ranged between -17.3‰ and 10.7‰ (mean = -14.2‰ , $n = 10$). Some of the most enriched $\Delta^{14}\text{C}$ -DIC values were measured at the stations farther from land at Transects T4 and T3. Since no samples were collected between 100 and 200 m depths for the remaining transects, we are unable to determine if this pattern was present throughout our study area. The most depleted $\Delta^{14}\text{C}$ signatures were measured at the two northernmost Transects T1 and T5 ($\Delta^{14}\text{C}$ -DIC = -28‰) and at the stations farthest from land in Transect T2 (Figure 3).

Surface water [DIC] ranged between 1,885 and 2,181 $\mu\text{mol/kg}$ (Figure S1). [DIC] smoothly increased from surface waters to reach the highest concentrations between 200 to 300 m before starting to decrease and remain $\sim 2,156 \mu\text{mol/kg}$ below 600 m. $[CO_2]$ ranged between 12 and 30 $\mu\text{mol/kg}$ (Figure 4). $[CO_2]$ maxima

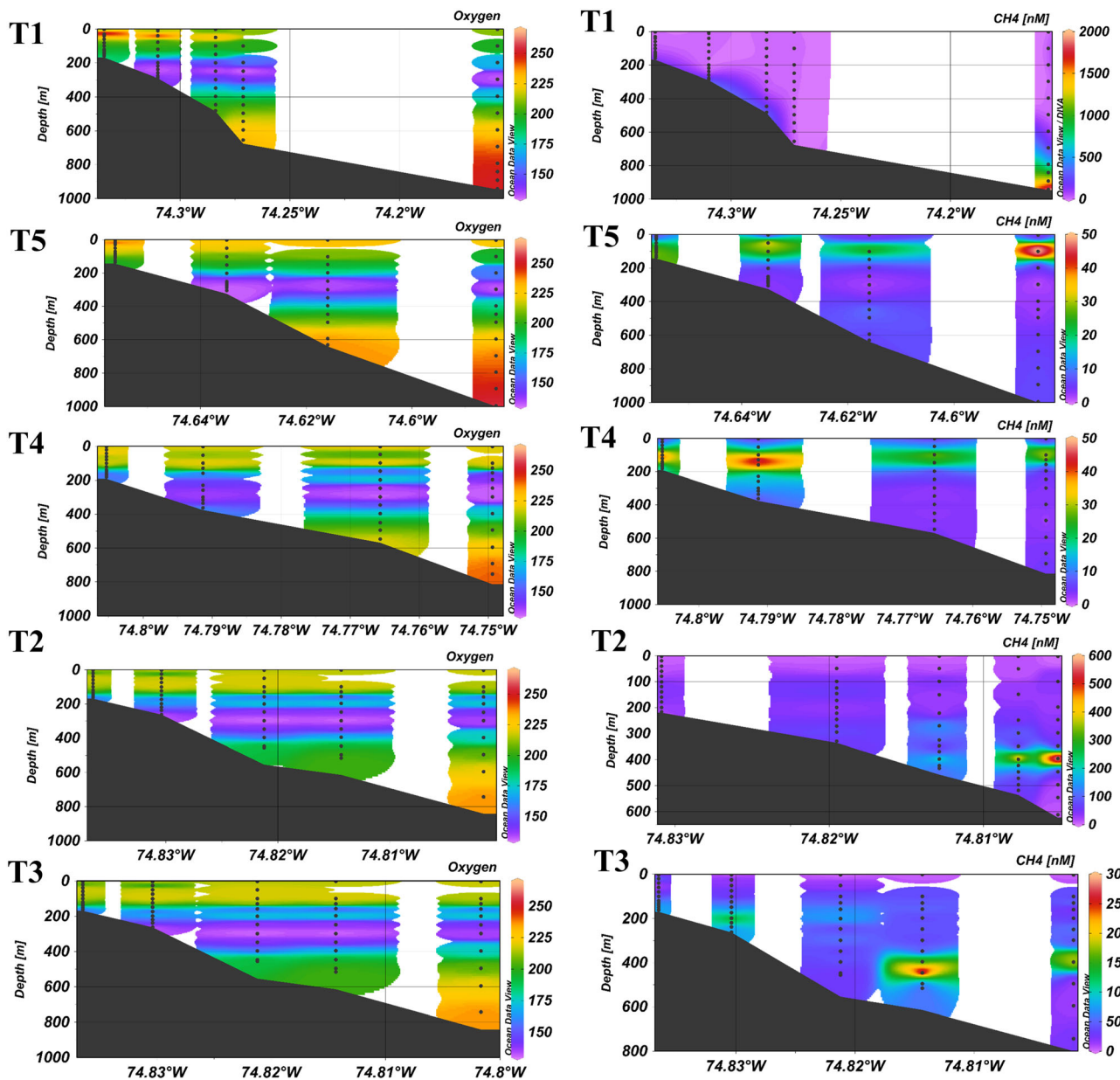


Figure 5. Distribution of dissolved oxygen ($\mu\text{mol/kg}$) on left and CH_4 concentration (nM) on right along sampled transects from most northerly (T1) to southerly (T3) transect. Note the different scale range for CH_4 concentration at each transect. Locations of discrete samples are indicated by black dots.

were observed between 200 and 400 m. Two maxima were observed at T2, a subsurface maximum at around 100 m and a deep maximum below 250 m. This transect also displayed the highest $[\text{CO}_2]$.

Seawater pH exhibited two minima at all transects except for T1 (Figure 4), one between 10 and 100 m depths (mean = 7.89, range = 7.83–8.04, $n = 39$) and a second one between 250 and 400 m (mean = 7.87, range = 7.84–7.91, $n = 56$). The shallow pH minimum coincided with elevated $[\text{CO}_2]$ and high subsurface bioscatter activity (Figures 3 and S2; see also EK60 data in Baldwin et al., 2020) suggesting that remineralization of suspended particles may be responsible for this pH signature (Hauri et al., 2009; Kwon et al., 2009). The deeper pH minimum at approximately 300 m was observed throughout the study area and agreed with high $[\text{CO}_2]$, ^{14}C -depleted $\Delta^{14}\text{C}$ -DIC, and the dissolved oxygen minimum (Figures 3–5). For water depths greater than 300 m, pH values at T1 and T5 were on average higher (7.93 at both transects) than at the

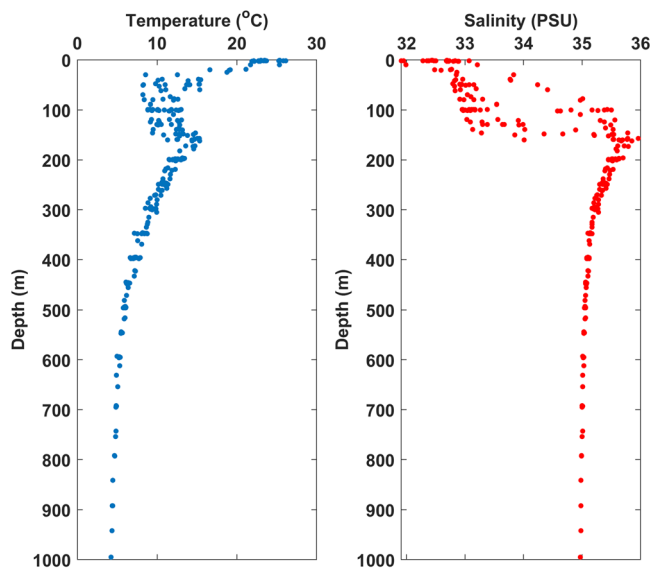


Figure 6. Temperature and salinity profiles measured during all CTD deployments.

southernmost transects (7.90–7.91). Among all transects, T2 consistently exhibited the lowest subsurface pH values (mean value 7.90).

Dissolved CH_4 concentrations along the MAB ranged from 1.3 to 2,108.1 nM and displayed high spatial variability both vertically and between stations (Figure 5). For water depths shallower than 10 m, an average CH_4 concentration of 4.2 nM (3.3–13.3 nM) was measured which is comparable to typical oceanic background levels (1–4 nM). The highest dissolved CH_4 concentrations were generally observed at water depths between 100 and 500 m, where concentrations reached 624.3 nM (mean value of 49.9 ± 80.1 nM). However, these elevated CH_4 values were not necessarily observed near the seafloor. For example, at Transect T2 the highest CH_4 concentrations were measured at 400 m depth, 223 m above the seafloor. Even though gas plumes were acoustically detected at all transects except for T4 (middle transect), CH_4 concentrations at T4 were above background and ranged between 2.6 and 42.9 nM. A more detailed description of CH_4 dynamics can be found in Leonte et al. (2020).

Samples for radiocarbon measurements of CH_4 dissolved in bottom waters near seeps show that CH_4 emitted from these features is fossil or nearly devoid of radiocarbon ($-968 \pm 34\%$, $n = 3$; Joung et al., 2018). We attribute the slight elevation above fossil to result from the sampling technique, which does not collect gas bubbles but rather CH_4 dissolved in seawater and may include background influences.

Different water current dynamics were observed between the northernmost (T1 and T5) and southernmost (T4, T2, and T3) transects (Figures 2 and S7). Currents between 100 and 200 m depths flowed southward along T1 (Figure 2) and T5 (Figure S4). The southward flowing MAB shelf water and northward flowing SAB shelf waters converged near Cape Hatteras forcing shelf water between 100 and 200 m northward at the T3, T2, and T4. For water depths between 350 and 450 m, ocean currents flow southward along Transect T1 and veer westward (inland) at T5 (Figures 2, S5, and S7). From the south, northward flowing SAB shelf waters converge near Cape Hatteras forcing shelf waters northwestward at T3, T2, and T4.

Surface temperature ranged between 21°C and 26°C (Figure 6). A temperature structure of cold water ($\sim 8^\circ\text{C}$) between two warm water layers was observed between 30 and 150 m except at T1 (Figure S9). Below 150 m, temperature increased to reach 15°C before starting to decrease again. Surface salinity ranged between 32 and 33 PSU (Figure 6). A halocline layer was also observed at about 200 m where salinity reached 36 PSU. Below 200 m depth, salinity became uniform at 35 PSU.

4. Discussion

The $\Delta^{14}\text{C}$ content of DIC in seawater is influenced by natural and anthropogenic carbon sources and is a useful tracer of physical and chemical processes. Exchange with atmospheric CO_2 dominates the distribution of $\Delta^{14}\text{C}$ -DIC in surface waters. In deeper waters $\Delta^{14}\text{C}$ -DIC is strongly influenced by other processes such as mixing of water masses with different $\Delta^{14}\text{C}$ -DIC signatures, the degradation of sinking organic carbon, and the oxidation of fossil CH_4 . Two trends are apparent in the $\Delta^{14}\text{C}$ data collected from the MAB (Figures 3 and S1). First, bomb $\Delta^{14}\text{C}$ is present in subsurface waters between 100 and 200 m with values ranging from 18‰ to 45‰. Second, the $\Delta^{14}\text{C}$ -DIC minimum at water depths between 350 and 450 m suggests that a source of old carbon is present and is influencing DIC. Here we discuss the potential sources of carbon that may explain the observed $\Delta^{14}\text{C}$ -DIC maxima at ~ 200 m water depth and the $\Delta^{14}\text{C}$ -DIC depletion at ~ 400 m.

4.1. Physical Processes Affecting Subsurface $\Delta^{14}\text{C}$ -DIC

General oceanic profiles of $\Delta^{14}\text{C}$ -DIC display an enrichment of $\Delta^{14}\text{C}$ in shallow waters, reflecting the penetration of anthropogenic radiocarbon generated by the atmospheric testing of nuclear weapons (i.e., bomb carbon). At greater depths, the $\Delta^{14}\text{C}$ signature of DIC becomes more depleted and uniform (Druffel

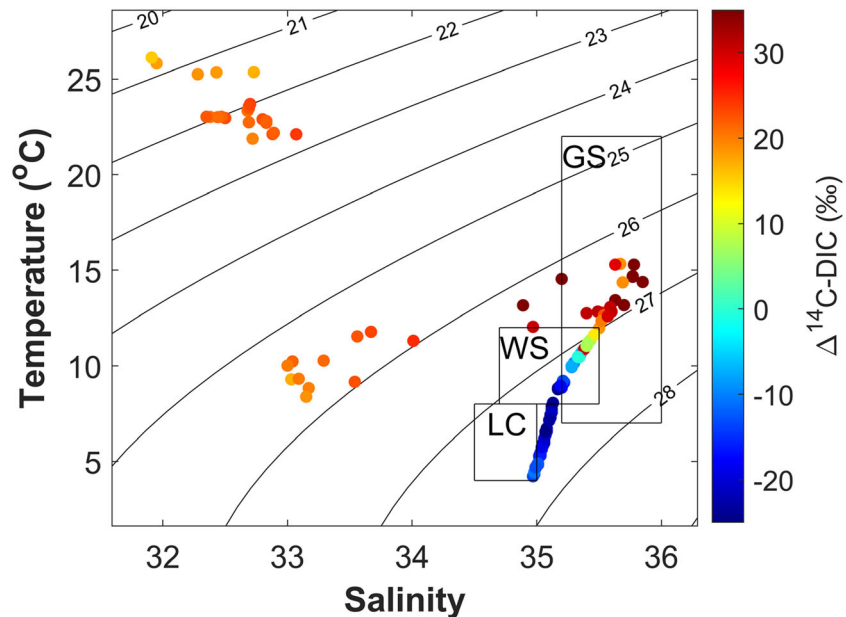


Figure 7. Temperature-salinity diagram for all measured $\Delta^{14}\text{C-DIC}$ data. Rectangles correspond to typical water mass characteristics for the Labrador Current (LC), Warm Slope Water (WS), and the Gulf Stream (GS). The color bar shows most enriched $\Delta^{14}\text{C-DIC}$ values are dominated by a water mass with Gulf Stream properties. Seawater density (kg/m^3) is indicated by the black contour lines.

et al., 2017; Gospodinova et al., 2016; McNichol et al., 1994). The $\Delta^{14}\text{C-DIC}$ maxima of 45‰ between 100 and 200 m depths at the southern transects (T4 and T3) indicate that bomb-enriched sources of $\Delta^{14}\text{C-DIC}$ are present. This depth range is below the observed diathermal layer (temperature structure of cold water between two warm water layers that acts as a physical barrier to vertical mixing; Figure 6). Thus, this maximum is unlikely to be directly caused by air-sea gas exchange. A significant moderate relationship between $\Delta^{14}\text{C-DIC}$ and O_2 for surface waters (Spearman coefficient $r = -0.5$, $p < 0.01$) suggests that this maximum may instead result from the remineralization of $\Delta^{14}\text{C}$ enriched organic carbon or mixing of water masses with a distinct $\Delta^{14}\text{C}$ signature.

Observations along the MAB have shown the shelf break and slope to receive the contribution of two main types of water masses: the deep Labrador Current, LC, (typically between 4°C and 8°C and with salinity 34.3–35) and the intermediate Warm Slope Water, WS, (typically between 8°C and 12°C and with salinity 34.7–35.5). Both water masses are relatively close to and dominated by the Gulf Stream (Fratantoni & Pickart, 2007; Gatién, 1976; Richaud et al., 2016; Wright & Parker, 1976). While the $\Delta^{14}\text{C-DIC}$ enrichment coincides with the salinity maxima (34.8–35.8) and warm subsurface temperatures (13–15°C), the observed temperature and salinity range is warmer and saltier than the characteristic Warm Slope Water. As shown in Figure 7, this $\Delta^{14}\text{C-DIC}$ enrichment mainly falls within temperature-salinity distributions characteristic of the Gulf Stream and may be explained by the input of water masses strongly influenced by the Gulf Stream (typical temperatures between 7°C and 22°C and salinity 35.2–36; Rasmussen et al., 2005). As revealed by Gula et al. (2019), it is possible for the Gulf Stream to be redistributed offshore of Cape Hatteras by subsurface submesoscale eddy-driven fluxes. This observation is supported by current models (Figure 2) and in situ measurements (Figures S4–S6), which reveal complex dynamics where the MAB and the South Atlantic Margin (SAB) waters meet. The southward flowing MAB shelf water and northward flowing SAB shelf waters converge near Cape Hatteras, forcing shelf water between 100 and 200 m northward (Figures 2 and S4). This suggests that the most plausible explanation for the subsurface $\Delta^{14}\text{C-DIC}$ maxima at the southernmost Transects T4 and T3 is mixing or the intrusion of water masses influenced by the Gulf Stream currents carrying a distinct $\Delta^{14}\text{C}$ signature. Bauer et al. (2002) investigated carbon cycling variability in the MAB, but different physical dynamics (Figure S8), sampling locations, and a sampling gap between 30 and 300 m, means that we are unable to use that data set as a reference. To our knowledge,

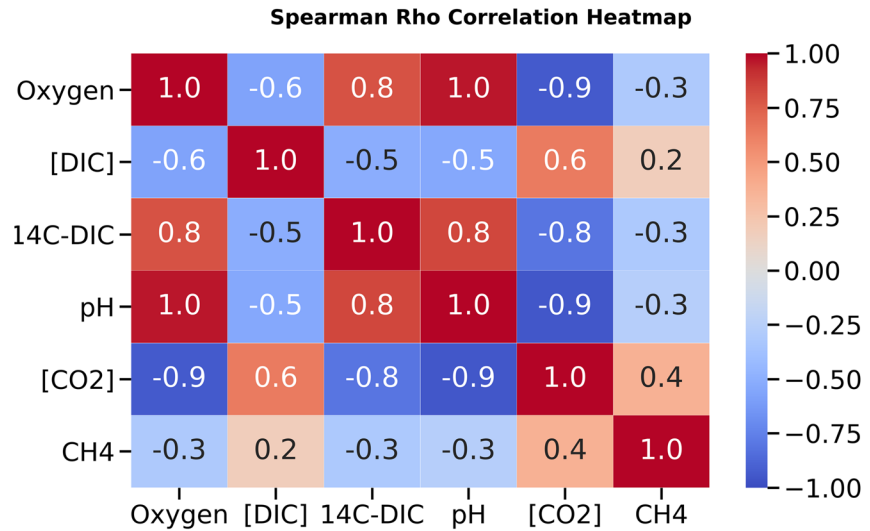


Figure 8. Spearman correlation heatmap for subsurface (>350 m) waters throughout the study area. Color bar shows Spearman's r value for each group of two variables. Darker colors indicate stronger correlations ($r = \pm 1$).

no other previous study that would allow us to characterize the signature of this Gulf Stream dominated Warm Slope Water mass has collected $\Delta^{14}\text{C}$ -DIC data in this region.

4.2. Ancient Methane as a Source of Depleted $\Delta^{14}\text{C}$

The $\Delta^{14}\text{C}$ -DIC minimum at T1, T5, and T2 suggests that an older source of carbon is influencing DIC at water depths greater than 350 m. This depth range coincided with the second subsurface pH minima, low dissolved oxygen, and high $[\text{CO}_2]$ (Figures 3–5). The strong to moderate correlation between pH, dissolved oxygen, $[\text{CO}_2]$, and $\Delta^{14}\text{C}$ -DIC (Figure 8) implies that this pH minimum may be caused by the remineralization of organic matter or the oxidation of CH_4 devoid of radiocarbon emitted from gas seeps (Bauer et al., 1990; Boudreau et al., 2015; Semiletov et al., 2016). Transects T1, T5, and T2 were located near gas seeps and associated with elevated CH_4 concentrations (Figures 1 and 5) and substantial oxidation (Leonte et al., 2020). However, due to the ephemeral nature of CH_4 seeps in this region (Skarke, 2015) and the strong spatial gradients in CH_4 concentration near bubble plumes (Leonte et al., 2018), the quantitative characterization of the correlation between $\Delta^{14}\text{C}$ -DIC and CH_4 is difficult. The advection of a water mass from the Gulf Stream can be discarded as possible source of depleted $\Delta^{14}\text{C}$ -DIC for the northernmost transects as currents flow south (Figure 2). The northwestward current flow at the southern transects could transport Gulf Stream waters, but temperature-salinity diagrams do not show inputs of Gulf Stream water at this depth (Figures 6 and S3). This suggests that physical processes alone cannot explain the $\Delta^{14}\text{C}$ minima.

The local contribution of oxidized ancient CH_4 on DIC is estimated using a radiocarbon mass balance model. The observed $\Delta^{14}\text{C}$ -DIC ($^{14}\text{C}_{\text{obs}}$) is considered a mixture of background seawater $\Delta^{14}\text{C}$ -DIC ($^{14}\text{C}_{\text{bkg}}$) and ancient $\Delta^{14}\text{C}$ -DIC ($^{14}\text{C}_{\text{anc}}$). The fraction of ancient carbon (f_{anc}) in $\Delta^{14}\text{C}$ -DIC is calculated by rearranging Equations 1 and 2:

$$^{14}\text{C}_{\text{obs}} = ^{14}\text{C}_{\text{bkgd}} \cdot f_{\text{bkgd}} + ^{14}\text{C}_{\text{anc}} \cdot f_{\text{anc}} \quad (1)$$

$$1 = f_{\text{Bkgd}} + f_{\text{anc}} \quad (2)$$

$^{14}\text{C}_{\text{obs}}$ was the measured $\Delta^{14}\text{C}$ -DIC for water depths greater than 350 m (i.e., the most depleted $\Delta^{14}\text{C}$ values). Since all transects had above background CH_4 concentrations, even where gas seeps were not detected (T4), we chose three different values for $^{14}\text{C}_{\text{bkg}}$ based on the observed $\Delta^{14}\text{C}$ -DIC water column distributions

$$\Sigma^{14}\text{C-DIC}_{\text{anc}} = \Sigma([\text{DIC}]_{\text{mean}} \times f_{\text{anc}} \times Z_{\text{s}} \times L_{\text{s}} \times Q_{\text{s}})_{\text{T}}$$

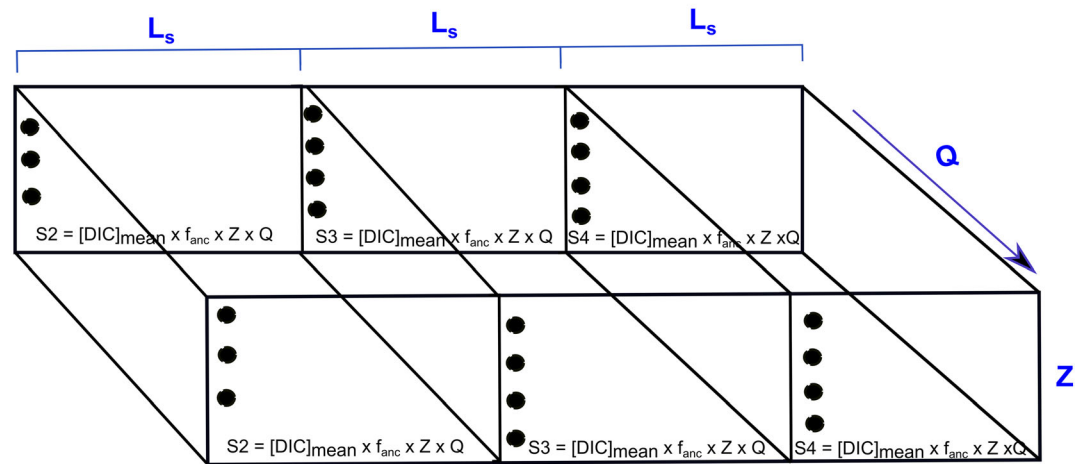


Figure 9. Diagram for calculating input rates of ancient DIC. Here L represents the distance between each station along a transect, Q is the in situ subsurface water velocity at depths >350 m, and Z is the water column depth between 350 m and the seafloor depth at each station. The black dots represent the depth at which samples were collected.

throughout this study area: -13% , -15% , and -17% . This range corresponds to the observed $\Delta^{14}\text{C-DIC}$ minimum (lower limit), average, and maximum (upper limit) for depths greater than 550 m (where the $\Delta^{14}\text{C-DIC}$ distribution becomes more uniform; Figure 3). Two $^{14}\text{C}_{\text{anc}}$ values are used, the measured $\Delta^{14}\text{C-CH}_4$ value of -968% and a fossil value assigned to be $-1,000\%$ (Kessler et al., 2008; Pohlman et al., 2010; Sparrow et al., 2018). No significant differences in the model results were obtained when using either $^{14}\text{C}_{\text{anc}}$ value. Therefore, the discussion will focus on results obtained using a fossil value instead of the measured $^{14}\text{C}_{\text{anc}}$ value because the latter one is likely to contain a mixture of both seep and background methane as indicated above. Model results are reported as the mean and standard deviation of f_{anc} estimated using the three different values for $^{14}\text{C}_{\text{bkg}}$.

Using these different values for $^{14}\text{C}_{\text{bkg}}$, the average estimated contribution of ancient methane-derived carbon to deep-seawater DIC was $0.5 \pm 0.4\%$ and ranged between $0.3 \pm 0.3\%$ (lower limit) and $0.7 \pm 0.4\%$ (upper limit). The largest fractions of $^{14}\text{C}_{\text{anc}}$ were calculated for samples collected at the northernmost Transects T1 and T5 (up to 1.6% for the upper limit). For T2 (second most southerly transect), mean f_{anc} values ranged between $0.5 \pm 0.2\%$ and $0.9 \pm 0.3\%$ (lower and upper limits). Although no gas seeps were detected at T4, f_{anc} for this transect ranged between $0.2 \pm 0.3\%$ and $0.5 \pm 0.4\%$. These results suggest that within the MAB, the influence of ancient CH_4 on DIC is more localized to areas where CH_4 concentrations are elevated and gas seepage is active, rather than displaying a cumulative effect down current to the south.

The radiocarbon model shows that the fraction of carbon from ancient CH_4 is small, which is consistent with the results from Hudson Canyon (Garcia-Tigreros & Kessler, 2018). However, like the uptake of anthropogenic CO_2 from the atmosphere, the oxidation of seep CH_4 -derived carbon may become more noticeable over decadal or longer time scales. Our data set allows us to compare the magnitude of these two sources of inorganic carbon (atmosphere and seeps) to seawater following a first-order approximation of the input rate of seep-derived DIC to these deeper waters ($\Sigma^{14}\text{C-DIC}_{\text{anc}}$; Figure 9). As observed from in situ current measurements (Figures S4–S6) and the USGS Coupled-Ocean-Atmosphere-Wave-Sediment-Transport model (Figure 2), complex physical dynamics are revealed throughout the study area. From the north, ocean currents flow southward along Transect T1 and veer westward (inland) at T5. From the south, northward flowing SAB shelf waters converge near Cape Hatteras forcing shelf waters northwestward at T3, T2, and T4. Since gas seeps have been detected south of the area covered in this study, it is possible that the north flowing SAB shelf waters carry $\Delta^{14}\text{C-DIC}$ depleted water at this depth. A first-order estimate of the input rate of ancient seep-derived DIC to this region is calculated assuming steady state and a dominating southerly current flow (Fratantoni & Pickart, 2007; Rasmussen et al., 2005). For this calculation, we incorporate the

measured [DIC] and the mean fraction of ancient carbon (f_{anc}) for each station. The $\Sigma^{14}\text{C-DIC}_{anc}$ for the study area is estimated by summing the inputs of $\Delta^{14}\text{C-DIC}_{anc}$ over all transects:

$$\Sigma^{14}\text{C-DIC}_{anc} = \sum ([\text{DIC}]_{\text{means}} \cdot f_{\text{ancs}} \cdot Z_s \cdot L_s \cdot Q_s)_T \quad (3)$$

where $[\text{DIC}]_{\text{mean}}$ is the average [DIC] at each station (s), Z (m) is the water column depth between 350 m and the seafloor at each station, f_{anc} is the mean fraction of ancient carbon for each station calculated using the model above, L (m) is the distance between each station along a transect T , and Q is the average subsurface (>350 m) current velocity at each station calculated from in situ LADCP data (Ruiz-Angulo et al., 2020).

A $\Sigma^{14}\text{C-DIC}_{anc}$ input rate of 2.2×10^{11} mol/yr is calculated over the 234 km of continental margin surveyed in this study. The calculated input rate is equivalent to 0.8% of the coastal ocean anthropogenic uptake of CO_2 (2.7×10^{13} mol/yr; Bourgeois et al. (2016)). An upper limit estimate for the northern U.S. Atlantic margin where gas seepage has been recognized (1,300 km; Skarke et al., 2014) suggests a $\Sigma^{14}\text{C-DIC}_{anc}$ input rate of 6.1×10^{11} mol/yr or 2.2% of the total coastal anthropogenic uptake of CO_2 . This input rate is higher than previous CH_4 emission estimates over gas seeps along the MAB ($0.95\text{--}5.66 \times 10^6$ mol/yr; Skarke et al., 2014) but falls within the global continental shelf approximation of 5.0×10^{11} and 4.1×10^{12} mol/yr (Hovland et al., 1993). Skarke et al. (2014) relied on observations of bubble characteristics at a few seeps to infer methane emissions and did not account for CH_4 diffusing from sediments, leading to conservative emission estimates. Recent acoustic data identified over 100 new active seep clusters along the MAB and indicate that CH_4 release may be more intense than originally expected (Skarke et al., 2018). In addition, Weinstein et al. (2016) estimated CH_4 input rates for a limited 32-km² area of Hudson Canyon to be 4.4×10^6 mol/yr, which is significantly above the estimates of Skarke et al. (2018) if extrapolated along the U.S. MAB and more in line with the estimates from this study. These reasons possibly contribute to the discrepancy in emission estimates. However, this disparity may also reflect the input and remineralization of other sedimentary sources of fossil carbon into bottom waters such as ancient CH_4 -derived dissolved organic carbon (Pohlman et al., 2010). Overall, the $\Delta^{14}\text{C}$ input rates presented here for the MAB suggest that if similar rates are found in other global continental margins, the oxidation of ancient carbon is not negligible on the global scale and could contribute to ocean acidification over longer time scales.

5. Conclusions

The $\Delta^{14}\text{C}$ distribution of DIC was assessed along the MAB. Within subsurface waters between 100 and 200 m, $\Delta^{14}\text{C-DIC}$ values range from 18‰ to 45‰, suggesting that bomb $\Delta^{14}\text{C}$ is being introduced, especially at the southernmost transects. Temperature-salinity diagrams along with current measurements indicate that the most plausible explanation for the subsurface $\Delta^{14}\text{C-DIC}$ maxima is mixing or the intrusion of water masses influenced by Gulf Stream currents carrying a distinct $\Delta^{14}\text{C}$ signature.

Bottom waters between 350 and 450 m displayed a layer of low $\Delta^{14}\text{C-DIC}$ at Transects T1, T5, and T2. The proximity of these transects to active gas seeps, the elevated CH_4 concentrations, and the substantial CH_4 oxidation (Leonte et al., 2020) suggest that CH_4 -derived CO_2 could be a source of fossil carbon. The average calculated contribution of ancient seep CH_4 -derived carbon to deep-seawater DIC ranged between $0.3 \pm 0.3\%$ and $0.7 \pm 0.4\%$ in the study area (mean value $0.5 \pm 0.4\%$). The largest fractions of ancient carbon (an upper estimate of up to 1.6%) were observed in samples from the northern part of the study area, where the transect crossed numerous seeps and elevated CH_4 concentrations were measured. Thus, the impacts of ancient CH_4 on DIC appeared greatest in localized areas where CH_4 concentrations are elevated. While our study investigated a distance of 234 km of the continental slope along the margin, if similar CH_4 seep emissions and oxidation rates are present throughout the U.S. Atlantic margin, a deepwater acidification effect equivalent to 2.2% of that caused by global infiltration of anthropogenic CO_2 in shallow waters may be occurring today. Since seep CH_4 input rates are likely to be heterogeneously distributed along other continental margins globally, similar studies on other ocean margins are needed to refine our understanding of this deep ocean acidification effect at the global scale. Nonetheless, this investigation along the U.S. MAB suggests the impact of aerobic CH_4 oxidation on ocean acidification could be significant globally.

Data Availability Statement

The data presented in this work can be found in the supporting information and can also be accessed at the NOAA's Nation Center for Environmental Information (<https://data.nodc.noaa.gov/cgi-bin/iso?id=gov.noaa.nodc:0209187>). LADCP data are available from Ruiz-Angulo et al. (2020), and geophysical data have been released by Baldwin et al. (2020).

Acknowledgments

This study was sponsored by U.S. Department of Energy (DE-FE0028980, awarded to J. D. K; DE-FE0026195 interagency agreement with C. D. R.). We thank the crew of the *R/V Hugh R. Sharp* for their support, G. Hatcher, J. Borden, and M. Martini of the USGS for assistance with the LADCP, and Zach Bunnell, Lillian Henderson, and Allison Laubach for additional support at sea. The quality of this manuscript was greatly improved thanks to the insightful comments of the two reviewers and P. Hart. Any use of trade, firm or product name is for descriptive purposes only and does not imply endorsement by the U.S. Government.

References

Alling, V., Porcelli, D., Mörth, C.-M., Anderson, L., Sanchez-Garcia, L., Gustafsson, Ö., et al. (2012). Degradation of terrestrial organic carbon, primary production and out-gassing of CO₂ in the Laptev and East Siberian Seas as inferred from δ¹³C values of DIC. *Geochimica et Cosmochimica Acta*, 95, 143–159. <http://doi.org/10.1016/j.gca.2012.07.028>

Andrews, B., Chaytor, J. D., ten Brink, U. S., Brothers, D. S., & Gardner, J. V. (2013). Bathymetric terrain model of the Atlantic margin for marine geological investigations. U.S. Geological Survey Open-File Report 2012–1266, <https://doi.org/10.3133/ofr20121266>

Archer, D., Buffett, B., & Brovkin, V. (2009). Ocean methane hydrates as a slow tipping point in the global carbon cycle. *Proceedings of the National Academy of Sciences*, 106(49), 20,596–20,601. <https://doi.org/10.1073/pnas.0800885105>

Baldwin, W. E., Moore, E. M., Worley, C. R., Nichols, A. R., & Ruppel, C. D. (2020). Marine geophysical data collected to support methane seep research along the U.S. Atlantic continental shelf break and upper continental slope between the Baltimore and Keller Canyons during U.S. Geological Survey Field Activities 2017-001-FA and 2017-002-FA: U.S. Geological Survey data release. <https://doi.org/10.5066/P9Y1MSTN>

Bauer, J. E., Druffel, E. R. M., Wolgast, D. M., & Griffin, S. (2002). Temporal and regional variability in sources and cycling of DOC and POC in the northwest Atlantic continental shelf and slope. *Deep Sea Research Part II: Topical Studies in Oceanography*, 49(20), 4387–4419. [https://doi.org/10.1016/S0967-0645\(02\)00123-6](https://doi.org/10.1016/S0967-0645(02)00123-6)

Bauer, J. E., Spies, R. B., Vogel, J. S., Nelson, D. E., & Southon, J. R. (1990). Radiocarbon evidence of fossil-carbon cycling in sediments of a nearshore hydrocarbon seep. *Nature*, 348(6298), 230–232. <http://doi.org/10.1038/348230a0>

Biaostoch, A., Treude, T., Rüpke, L. H., Riebesell, U., Roth, C., Burwicz, E. B., et al. (2011). Rising Arctic Ocean temperatures cause gas hydrate destabilization and ocean acidification. *Geophysical Research Letters*, 38, L08602. <https://doi.org/10.1029/2011GL047222>

Boudreau, B. P., Luo, Y., Meysman, F. J. R., Middelburg, J. J., & Dickens, G. R. (2015). Gas hydrate dissociation prolongs acidification of the Anthropocene oceans. *Geophysical Research Letters*, 42, 9337–9344A. <https://doi.org/10.1002/2015GL065779>

Bourgeois, T., Orr, J. C., Resplandy, L., Terhaar, J., Ethé, C., Gehlen, M., & Bopp, L. (2016). Coastal-ocean uptake of anthropogenic carbon. *Biogeosciences*, 13(14), 4167–4185. <https://doi.org/10.5194/bg-13-4167-2016>

Broecker, W. S., Takahashi, T., Simpson, H., & Peng, T.-H. (1979). Fate of fossil fuel carbon dioxide and the global carbon budget. *Science*, 206(4417), 409–418. <https://doi.org/10.1126/science.206.4417.409>

Brothers, D. S., Ruppel, C., Kluesner, J. W., ten Brink, U. S., Chaytor, J. D., Hill, J. C., et al. (2014). Seabed fluid expulsion along the upper slope and outer shelf of the U.S. Atlantic continental margin. *Geophysical Research Letters*, 41, 96–101. <https://doi.org/10.1002/2013GL058048>

Cai, W. J., Hu, X., Huang, W. J., Murrell, M. C., Lehrter, J. C., Lohrenz, S. E., et al. (2011). Acidification of subsurface coastal waters enhanced by eutrophication. *Nature Geoscience*, 4(11), 766–770. <https://doi.org/10.1038/NNGEO1297>

Canadell, J. G., Le Quéré, C., Raupach, M. R., Field, C. B., Buitenhuis, E. T., Ciais, P., et al. (2007). Contributions to accelerating atmospheric CO₂ growth from economic activity, carbon intensity, and efficiency of natural sinks. *Proceedings of the National Academy of Sciences*, 104(47), 18,866–18,870. <https://doi.org/10.1073/pnas.0702737104>

Chan, E. W., Shiller, A. M., Joung, D. J., Arrington, E. C., Valentine, D. L., Redmond, M. C., et al. (2019). Investigations of aerobic methane oxidation in two marine seep environments: Part 1—Chemical kinetics. *Journal of Geophysical Research: Oceans*, 124, 8852–8868. <https://doi.org/10.1029/2019JC015594>

Ciais, P., Sabine, C., Bala, G., Bopp, L., Brovkin, V., Canadell, J., et al. (2013). Carbon and other biogeochemical cycles. In T. F. Stocker et al. (Eds.), *Climate change 2013: The physical science basis. Contribution of Working Group I to the Fifth Assessment Report of the Intergovernmental Panel on Climate Change* (pp. 465–570). Cambridge, United Kingdom and New York, NY, USA: Cambridge University Press.

Clayton, T. D., & Byrne, R. H. (1993). Spectrophotometric seawater pH measurements: Total hydrogen ion concentration scale calibration of m-cresol purple and at-sea results. *Deep Sea Research Part I: Oceanographic Research Papers*, 40(10), 2115–2129. <https://doi.org/10.1017/CBO9781107415324.015>

Dickens, G. R. (2003). Rethinking the global carbon cycle with a large, dynamic and microbially mediated gas hydrate capacitor. *Earth and Planetary Science Letters*, 213(3–4), 169–183. [https://doi.org/10.1016/S0012-821X\(03\)00325-X](https://doi.org/10.1016/S0012-821X(03)00325-X)

Dickens, G. R., O'Neil, J. R., Rea, D. K., & Owen, R. M. (1995). Dissociation of oceanic methane hydrate as a cause of the carbon isotope excursion at the end of the Paleocene. *Paleoceanography*, 10(6), 965–971. <https://doi.org/10.1029/95PA02087>

Dickson, A. G., Sabine, C. L., & Christian, J. R. (Eds.) (2007). *Guide to best practices for ocean CO₂ measurements, PICES Special Publication 3* (191 pp.). Retrieved from https://www.ncei.noaa.gov/access/ocean-carbon-data-system/oceans/Handbook_2007.html

Doney, S. C., Fabry, V. J., Feely, R. A., & Kleypas, J. A. (2009). Ocean acidification: the other CO₂ problem. *Annual Review of Marine Science*, 1(1), 169–192. <https://doi.org/10.1146/annurev.marine.010908.163834>

Druffel, E., Griffin, S., Glynn, C., Benner, R., & Walker, B. (2017). Radiocarbon in dissolved organic and inorganic carbon of the Arctic Ocean. *Geophysical Research Letters*, 44, 2369–2376. <https://doi.org/10.1002/2016GL072138>

Du, M., & Kessler, J. D. (2012). Assessment of the spatial and temporal variability of bulk hydrocarbon respiration following the Deepwater Horizon oil spill. *Environmental Science & Technology*, 46(19), 10,499–10,507. <https://doi.org/10.1021/es301363k>

Feely, R. A., Alin, S. R., Newton, J., Sabine, C. L., Warner, M., Devol, A., et al. (2010). The combined effects of ocean acidification, mixing, and respiration on pH and carbonate saturation in an urbanized estuary. *Estuarine, Coastal and Shelf Science*, 88(4), 442–449. <http://www.sciencedirect.com/science/article/pii/S027277141000185X>, <https://doi.org/10.1016/j.ecss.2010.05.004>

Feely, R. A., Doney, S. C., & Cooley, S. R. (2009). Ocean acidification: Present conditions and future changes in a high-CO₂ world. *Oceanography*, 22(4), 36–47. <https://doi.org/10.5670/oceanog.2009.95>

- Feely, R. A., Sabine, C. L., Lee, K., Berelson, W., Kleypas, J., Fabry, V. J., & Millero, F. J. (2004). Impact of anthropogenic CO₂ on the CaCO₃ system in the oceans. *Science*, 305(5682), 362–366. <http://science.sciencemag.org/content/sci/305/5682/362.full.pdf>, <https://doi.org/10.1126/science.1097329>
- Fratantoni, P. S., & Pickart, R. S. (2007). The western North Atlantic shelfbreak current system in summer. *Journal of Physical Oceanography*, 37(10), 2509–2533. <https://doi.org/10.1175/JPO3123.1>
- Gao, P., Xu, X., Zhou, L., Pack, M. A., Griffin, S., Santos, G. M., et al. (2014). Rapid sample preparation of dissolved inorganic carbon in natural waters using a headspace-extraction approach for radiocarbon analysis by accelerator mass spectrometry. *Limnology and Oceanography: Methods*, 12(4), 174–190. <https://doi.org/10.4319/lom.2014.12.174>
- Garcia-Tigreros, F., & Kessler, J. D. (2018). Limited acute influence of aerobic methane oxidation on ocean carbon dioxide and pH in Hudson Canyon, Northern U.S. Atlantic Margin. *Journal of Geophysical Research: Biogeosciences*, 123, 2135–2144. <https://doi.org/10.1029/2018JG004384>
- Gatien, M. G. (1976). A study in the slope water region south of Halifax. *Journal of the Fisheries Research Board of Canada*, 33(10), 2213–2217. <https://doi.org/10.1139/f76-270>
- Gospodinova, K., McNichol, A. P., Gagnon, A., & Walter, S. S. (2016). Rapid extraction of dissolved inorganic carbon from seawater and groundwater samples for radiocarbon dating. *Limnology and Oceanography: Methods*, 14(1), 24–30. <https://doi.org/10.1002/lom3.10066>
- Gula, J., Blacic, T. M., & Todd, R. E. (2019). Submesoscale coherent vortices in the Gulf Stream. *Geophysical Research Letters*, 46, 2704–2714. <https://doi.org/10.1029/2019GL081919>
- Hauri, C., Gruber, N., Plattner, G. K., Alin, S., Feely, R. A., Hales, B., & Wheeler, P. A. (2009). Ocean acidification in the California current system. *Oceanography*, 22(4), 60–71. <https://doi.org/10.5670/oceanog.2009.97>
- Hovland, M., Judd, A. G., & Burke, R. A. Jr. (1993). The global flux of methane from shallow submarine sediments. *Chemosphere*, 26(1–4), 559–578. [https://doi.org/10.1016/0045-6535\(93\)90442-8](https://doi.org/10.1016/0045-6535(93)90442-8)
- Joung, DongJoo, Leonte, M., Garcia-Tigreros, F., Ruppel, C. D., Kessler, J. D. (2018). Radiocarbon measurements of methane dissolved in seawater near the upper edge of methane hydrate stability, Natural Gas Hydrate Systems Gordon Research Conference, February 25, 2018 - March 02, 2018, TX United States.
- Kennett, J., & Stott, L. (1991). Abrupt deep sea warming, paleoceanographic changes and benthic extinctions at the end of the Paleocene. *Nature*, 353(6341), 225–229. <https://doi.org/10.1038/353225a0>
- Kessler, J. D., Reeburgh, W. S., Valentine, D. L., Kinnaman, F. S., Peltzer, E. T., Brewer, P. G., et al. (2008). A survey of methane isotope abundance (¹⁴C, ¹³C, ²H) from five nearshore marine basins that reveals unusual radiocarbon levels in subsurface waters. *Journal of Geophysical Research*, 113, C12021. <https://doi.org/10.1029/2008JC004822>
- Kessler, J. D., Valentine, D. L., Redmond, M. C., Du, M., Chan, E. W., Mendes, S. D., et al. (2011). A persistent oxygen anomaly reveals the fate of spilled methane in the deep Gulf of Mexico. *Science*, 331(6015), 312–315. <https://doi.org/10.1126/science.1199697>
- Krey, V., Canadell, J. G., Nakicenovic, N., Abe, Y., Andruleit, H., Archer, D., et al. (2009). Gas hydrates: entrance to a methane age or climate threat? *Environmental Research Letters*, 4(3), 034007. <https://doi.org/10.1088/1748-9326/4/3/034007>
- Kvenvolden, K. A. (1988). Methane hydrates and global climate. *Global Biogeochemical Cycles*, 2(3), 221–229. <https://doi.org/10.1029/GB002i003p00221>
- Kvenvolden, K. A., Lorenson, T. D., & Reeburgh, W. S. (2001). Attention turns to naturally occurring methane seepage. *Eos, Transactions American Geophysical Union*, 82(40), 457–457. <https://doi.org/10.1029/01EO00275>
- Kwon, E. Y., Primeau, F., & Sarmiento, J. L. (2009). The impact of remineralization depth on the air–sea carbon balance. *Nature Geoscience*, 2(9), 630–635. <https://doi.org/10.1038/NGEO612>
- Lamarque, J. F. (2008). Estimating the potential for methane clathrate instability in the 1%-CO₂ IPCC AR-4 simulations. *Geophysical Research Letters*, 35, L19806. <https://doi.org/10.1029/2008GL035291>
- Leonte, M., Kessler, J. D., Kellermann, M. Y., Arrington, E. C., Valentine, D. L., & Sylva, S. P. (2017). Rapid rates of aerobic methane oxidation at the feather edge of gas hydrate stability in the waters of Hudson Canyon, US Atlantic Margin. *Geochimica et Cosmochimica Acta*, 204, 375–387. <https://doi.org/10.1016/j.gca.2017.01.009>
- Leonte, M., Ruppel, C. D., Ruiz-Angulo, A., & Kessler, J. D. (2020). Surface methane concentrations along the Mid-Atlantic Bight driven by aerobic subsurface production rather than seafloor gas seeps. *Journal of Geophysical Research: Oceans*, 125, e2019JC015989. <https://doi.org/10.1029/2019JC015989>
- Leonte, M., Wang, B., Socolofsky, S. A., Mau, S., Breier, J. A., & Kessler, J. D. (2018). Using carbon isotope fractionation to constrain the extent of methane dissolution into the water column surrounding a natural hydrocarbon gas seep in the northern Gulf of Mexico. *Geochemistry, Geophysics, Geosystems*, 19, 4459–4475. <https://doi.org/10.1029/2018GC007705>
- Liu, X., Patsavas, M. C., & Byrne, R. H. (2011). Purification and characterization of meta-cresol purple for spectrophotometric seawater pH measurements. *Environmental Science & Technology*, 45(11), 4862–4868. <https://doi.org/10.1021/es200665d>
- Mau, S., Heintz, M. B., & Valentine, D. L. (2012). Quantification of CH₄ loss and transport in dissolved plumes of the Santa Barbara Channel, California. *Continental Shelf Research*, 32, 110–120. <https://doi.org/10.1016/j.csr.2011.10.016>
- McGinnis, D. F., Greinert, J., Artemov, Y., Beaubien, S. E., & Wuest, A. (2006). Fate of rising methane bubbles in stratified waters: How much methane reaches the atmosphere? *Journal of Geophysical Research*, 111, C09007. <https://doi.org/10.1029/2005JC003183>
- McNichol, A., Jones, G., Hutton, D., Gagnon, A., & Key, R. (1994). The rapid preparation of seawater ΣCO₂ for radiocarbon analysis at the National Ocean Sciences AMS Facility. *Radiocarbon*, 36(2), 237–246. <https://doi.org/10.1017/S0033822200040522>
- Orr, J. C., Fabry, V. J., Aumont, O., Bopp, L., Doney, S. C., Feely, R. A., et al. (2005). Anthropogenic ocean acidification over the twenty-first century and its impact on calcifying organisms. *Nature*, 437(7059), 681–686. <https://doi.org/10.1038/nature04095>
- Pack, M. A., Xu, X., Lupascu, M., Kessler, J. D., & Czimczik, C. I. (2015). A rapid method for preparing low volume CH₄ and CO₂ gas samples for ¹⁴C AMS analysis. *Organic Geochemistry*, 78, 89–98. <https://doi.org/10.1016/j.orggeochem.2014.10.010>
- Phrampus, B. J., & Hornbach, M. J. (2012). Recent changes to the Gulf Stream causing widespread gas hydrate destabilization. *Nature*, 490(7421), 527–530. <https://doi.org/10.1038/nature11528>
- Pohlman, J. W., Bauer, J. E., Waite, W. F., Osburn, C. L., & Chapman, N. R. (2010). Methane hydrate-bearing seeps as a source of aged dissolved organic carbon to the oceans. *Nature Geoscience*, 4(1), 37–41. <https://doi.org/10.1038/ngeo1016>
- Quay, P. D., Tilbrook, B., & Wong, C. S. (1992). Oceanic uptake of fossil fuel CO₂: Carbon-13 evidence. *Science*, 256(5053), 74–79. <https://doi.org/10.1126/science.256.5053.74>
- Rasmussen, L. L., Gawarkiewicz, G., & Owens, W. B. (2005). Slope water, Gulf Stream, and seasonal influences on southern Mid-Atlantic Bight circulation during the fall-winter transition. *Journal of Geophysical Research*, 110, C02009. <https://doi.org/10.1029/2004JC002311>

- Richaud, B., Kwon, Y. O., Joyce, T. M., Fratantoni, P. S., & Lentz, S. J. (2016). Surface and bottom temperature and salinity climatology along the continental shelf off the Canadian and US East Coasts. *Continental Shelf Research*, *124*, 165–181. <https://doi.org/10.1016/j.csr.2016.06.005>
- Ruiz-Angulo, A., Ruppel, C. D., Hatcher, G., & Kessler, J. D. (2020). Current velocities as a function of depth measured by lowered ADCP (LADCP) on the R/V Hugh R. Sharp in the Mid-Atlantic Bight from 2017-08-25 to 2017-09-03. Retrieved from NOAA National Centers for Environmental Information. <https://accession.nodc.noaa.gov/0209236>
- Ruppel, C. D. (2011). Methane Hydrates and Contemporary Climate Change. *Nature Education Knowledge*, *3*(10), 29.
- Ruppel, C. D., & Kessler, J. D. (2017). The interaction of climate change and methane hydrates. *Reviews of Geophysics*, *55*, 126–168. <https://doi.org/10.1002/2016RG000534>
- Semiletov, I., Pipko, I., Gustafsson, Ö., Anderson, L. G., Sergienko, V., Pugach, S., et al. (2016). Acidification of East Siberian Arctic Shelf waters through addition of freshwater and terrestrial carbon. *Nature Geoscience*, *9*(5), 361–365. <https://doi.org/10.1038/ngeo2695>
- Skarke, A. (2015). New insights into the temporal variability of seafloor methane discharge on the northern US Atlantic margin. AGU Fall Meeting.
- Skarke, A., Ruppel, C., Kidiwela, M., & Baldwin, W. (2018). Expanded US Atlantic Margin seep inventory yields insight into methane dynamics. AGU Fall Meeting.
- Skarke, A., Ruppel, C., Kodis, M., Brothers, D., & Lobecker, E. (2014). Widespread methane leakage from the sea floor on the northern US Atlantic margin. *Nature Geoscience*, *7*(9), 657–661. <https://doi.org/10.1038/NNGEO2232>
- Sparrow, K. J., Kessler, J. D., Southon, J. R., Garcia-Tigreros, F., Schreiner, K. M., Ruppel, C. D., et al. (2018). Limited contribution of ancient methane to surface waters of the US Beaufort Sea shelf. *Science Advances*, *4*(1), eaao4842. <https://doi.org/10.1126/sciadv.aao4842>
- Stranne, C., O'Regan, M., & Jakobsson, M. (2016). Overestimating climate warming-induced methane gas escape from the seafloor by neglecting multiphase flow dynamics. *Geophysical Research Letters*, *43*, 8703–8712. <https://doi.org/10.1002/2016GL070049>
- Sunda, W. G., & Cai, W.-J. (2012). Eutrophication induced CO₂-acidification of subsurface coastal waters: Interactive effects of temperature, salinity, and atmospheric pCO₂. *Environmental Science & Technology*, *46*(19), 10,651–10,659. <https://doi.org/10.1021/es300626f>
- Thurnherr, A. M. (2011). How to process LADCP data with the LDEO software. Versions IX.7-IX.10. https://www.bodc.ac.uk/data/documents/nodb/pdf/ladcp_ideo_processing_IX.7_IX.10.pdf
- Valentine, D. L., Blanton, D. C., Reeburgh, W. S., & Kastner, M. (2001). Water column methane oxidation adjacent to an area of active hydrate dissociation, Eel River Basin. *Geochimica et Cosmochimica Acta*, *65*(16), 2633–2640. [https://doi.org/10.1016/S0016-7037\(01\)00625-1](https://doi.org/10.1016/S0016-7037(01)00625-1)
- Van Heuven, S., Pierrot, D., Rae, J. W. B., Lewis, E., & Wallace, D. W. R. (2011). MATLAB Program developed for CO₂ system calculations. In *ORNL/CDIAC-105b, Carbon Dioxide Information Analysis Center*. Oak Ridge, TN: Oak Ridge National Laboratory, U.S. Department of Energy. https://doi.org/10.3334/CDIAC/otg.CO2SYS_MATLAB_v1.1
- Warner, J., Armstrong, B., He, R., & Zambon, J. (2010). Development of a Coupled Ocean-Atmosphere-Wave-Sediment Transport (COAWST) modeling system. *Ocean Modelling*, *35*(3), 230–244. <https://doi.org/10.1016/j.ocemod.2010.07.010>
- Weinstein, A., Navarrete, L., Ruppel, C., Weber, T. C., Leonte, M., Kellermann, M. Y., et al. (2016). Determining the flux of methane into Hudson Canyon at the edge of methane clathrate hydrate stability. *Geochemistry, Geophysics, Geosystems*, *17*, 3882–3892. <https://doi.org/10.1002/2016GC006421>
- Wright, W. R., & Parker, C. E. (1976). A volumetric temperature/salinity census for the Middle Atlantic Bight. *Limnology and Oceanography*, *21*(4), 563–571. <https://doi.org/10.4319/lo.1976.21.4.0563>
- Zachos, J. C., Röhl, U., Schellenberg, S. A., Sluijs, A., Hodell, D. A., Kelly, D. C., et al. (2005). Rapid acidification of the ocean during the Paleocene-Eocene thermal maximum. *Science*, *308*(5728), 1611–1615. <https://doi.org/10.1126/science.1109004>
- Zeebe, R. E., Ridgwell, A., & Zachos, J. C. (2016). Anthropogenic carbon release rate unprecedented during the past 66 million years. *Nature Geoscience*, *9*(4), 325. <https://doi.org/10.1038/ngeo2681>